Welding Simulation in Advanced Manufacturing and Design of Steel Structures

Theses of dissertation

Department of Structural Engineering
Faculty of Civil Engineering
Budapest University of Technology and Economics

Dénes Kollár

Supervisor
Balázs Géza Kövesdi, PhD

Budapest
2020

Table of contents

7 Future research work

A range of related topics are proposed for further studies using the same finite element framework developed for virtual manufacturing and virtual testing such as:

- performing stochastic analyses in order to focus on the differences of manual and robotic welding and determine the influence of probability-based welding variables, varying in time, on welding-induced imperfections and structural resistance,
- developing and refining residual stress models using finite element method for welded steel structures widely used in the civil engineering practice, e.g. corrugated web girders,
- developing equivalent geometric imperfections for shear buckling of corrugated web girders considering geometric imperfections and residual stresses for simulation-based design,
- developing buckling curves, performing both stochastic virtual manufacturing and virtual testing and assuming dimensional data, material properties and welding variables as probabilistic variables in simulations.

6.2 Relevant publications

Academic journal articles:

[DK1] D. Kollár, B. Kövesdi, L.G. Vigh, S. Horváth, Weld process model for simulating metal active gas welding, International Journal of Advanced Manufacturing Technology. 102(5-8) (2019) 2063–2083. doi:10.1007/s00170-019-03302-3. **Impact factor: 2.496**

[DK2] D. Kollár, B. Kövesdi, Welding simulation of corrugated web girders - Part 1: Effect of manufacturing on residual stresses and imperfections, Thin-Walled Structures. 146 (2020) 106107. doi:10.1016/j.tws.2019.04.006. **Impact factor: 3.488**

[DK3] D. Kollár, B. Kövesdi, Welding simulation of corrugated web girders - Part 2: Effect of manufacturing on shear buckling resistance, Thin-Walled Structures. 141 (2019) 477–488. doi:10.1016/j.tws.2019.04.035. **Impact factor: 3.488**

[DK4] B. Somodi, D. Kollár, B. Kövesdi, J. Néző, L. Dunai, Residual stresses in high-strength steel welded square box sections, Proceedings of the Institution of Civil Engineers: Structures and Buildings. 170 (2017) 804–812. doi:10.1680/jstbu.16.00139. **Impact factor: 0.877**

[DK5] D. Kollár, B. Kövesdi, J. Néző, Numerical simulation of welding process – Application in buckling analysis, Periodica Polytechnica Civil Engineering. 61 (2017) 98–109. doi:http://dx.doi.org/10.3311/PPci.9257. **Impact factor: 0.976**

Conference papers:

[DK6] V. Budaházy, D. Kollár, L.G. Vigh, Simulation based imperfections and their effects on stability resistance, in: F. Wald, M. Jandera (Eds.), Stability and Ductility of Steel Structures 2019: Proceedings of the International Colloquia on Stability and Ductility of Steel Structures, CRC Press, Leiden, 2019: pp. 205–212.

[DK7] D. Kollár, B. Kövesdi, Validation of heat source model for metal active gas welding, in: C. Sommitsc, N. Enzinger, P. Mayr (Eds.), Mathematical Modelling of Weld Phenomena 12, Verlag der Technischen Universität Graz, Deutschlandsberg, Austria, 2018: pp. 53–80. doi:10.3217/978-3-85125-615-4-05.

[DK8] D. Kollár, B. Kövesdi, Effect of imperfections and residual stresses on the shear buckling resistance of corrugated web girders, in: D. Camotim, N. Silvestre (Eds.), Proceedings of the Eighth International Conference on Thin Walled Structures, Lisbon, 2018: p. 20.

[DK9] D. Kollár, B. Kövesdi, Experimental and numerical simulation of welded columns, in: B. Bauer, I. Garasic (Eds.), Proceedings of 41st International Conference Zavarivanje – Welding 2016 - Opatija, Croatia, Hrvatsko Drustvo Za Tehniku Zavarivanja/Croatian Welding Society, Zagreb, 2016: pp. 123–132.

[DK10] D. Kollár, B. Kövesdi, Numerical Simulation of Welding Process, in: Young Welding Professionals International Conference, YPIC2015, Budapest, 2015: p. 6.

1 Introduction

1.1 Problem statement

Validated virtual manufacturing (i.e., manufacturing simulations) and virtual testing (i.e., buckling analysis, fatigue analysis, etc.) could be used for optimization and development purposes in accordance with a reduced number of experiments and tests on actual prototypes. In-process control methods and post-weld corrective methods can be modelled either to perform distortion-controlled or residual stress-controlled design. Numerous previous research activities highlighted the importance of residual stresses and geometric imperfections regarding the load bearing capacity of structural elements. However, most of the standards give only approximations and assumptions on equivalent geometric imperfections while the real structural behaviour can be significantly different. The current research program investigates and evaluates the advantages of virtual manufacturing and virtual testing of different welded steel products.

1.2 Motivation

Dissertation focuses on three different research topics in the field of advanced manufacturing and design of steel structures using numerical simulations consisting of virtual manufacturing and virtual testing. First research aim is to develop a validated numerical modelling framework to simulate arc welding processes using a general-purpose finite element software in order to predict temperature, stress and deformation fields during welding. Additional aim is to consider welding-induced imperfections based on welding simulations in geometrically and materially nonlinear analyses with imperfections (GMNIA) for improving the reliability of welded structures.

Second research objective is related to the development of a weld process model, using three-dimensional heat transfer model and double ellipsoidal heat source model, for typical welded joints taking welding variables and filler wire types into account in virtual manufacturing processes. Application of the developed numerical modelling tool can significantly reduce manufacturing costs by eliminating the need for post-weld corrective methods and efficiently enhance service life.

Steel I-girders with corrugated webs are in the focus of the third research topic. This girder type has been increasingly used in the past decades for bridges. Nevertheless, there are several specialities in their structural behaviour (e.g., ‘accordion effect’ due to negligible axial stiffness) which needs further investigation. The purpose of the current research is to evaluate typical residual stress distributions in trapezoidal corrugated web girders using manufacturing simulations and to analyse and evaluate the effect of imperfections on shear buckling resistance.

2 Research strategy

1 Development of finite element framework. Literature review is executed to investigate previous research activities conducted by researchers in the field of welding simulation. The developed finite element framework is presented for simulating arc welding processes in order to predict temperature, stress and deformation fields during welding. Implementation of uncoupled transient thermo-metallurgical-mechanical analysis and simplified approaches are discussed and studied. An automated Frenet-Serret frame is developed in order to simulate any arbitrary three-dimensional welding trajectory and movement of a local coordinate system representing the heat source. Details of GMNIA with realistic manufacturing-induced imperfections are investigated and implemented.

2 Development of weld process model. First, a comprehensive literature review related to heat source and weld process models is conducted. An extensive research program is carried out on small-scale specimens using different weld types, filler wire types, number of weld passes and welding variables. The experimental research program contains temperature measurements during welding, macrographs and deformation measurements after welding. The research program focuses on the relationship of welding variables and double ellipsoidal heat source model parameters. The numerical model is validated based on large number of experimental data. The developed weld process model provides heat source model parameters as a function of net heat input and it is applicable for a metal active gas welding power source and two electrode types.

3 Virtual buckling tests of trapezoidal corrugated web girders. Previous research activities related to residual stresses in corrugated web girders and shear buckling resistance are discussed. An experimental and numerical study is performed focusing on the evolution of total strains in corrugated web girders. The developed finite element model for welding simulation is validated based on strain gauge measurements, while the typical welding-induced longitudinal residual stresses in the web and flanges are determined. Simulated residual stress pattern of corrugated web girders is compared with conventional I-girders with flat web and the influence of 'accordion effect' during manufacturing is evaluated and determined. Virtual shear buckling tests are carried out taking manufacturing-induced imperfections into account. Results are compared with design formulae, differences are determined and evaluated.

flat web I-girders. Results demonstrate that the residual stress distribution for corrugated web girders and conventional I-girders are significantly different due to 'accordion effect' and different welding trajectories. Mainly membrane residual stresses are typical for girders with flat web, while bending residual stresses dominate for corrugated web girders. Membrane residual stresses are negligible in the web for corrugated web girders, except in the vicinity of the weld.

b) Typical residual stress distributions are presented for three different corrugation profiles; which results are compared with conventional flat web girders. Results demonstrate that there is a significant transverse bending moment in the flanges of corrugated web girders due to manufacturing, which increases compressive residual stresses.

c) Magnitude of tensile residual stresses within the flange and the web of a corrugated web girder is similar to flat web girders. Results demonstrate that tensile zone width of the residual stress pattern in the web is independent from corrugation angle.

Related publications: **[DK2] & [DK8]**

Thesis 5. Shear buckling resistance of corrugated web girders are determined using equivalent geometric imperfections and virtual tests considering virtual manufacturing-based residual stresses and geometric imperfections due to cold forming, thermal cutting and welding. Comparison of numerical results shows that using equivalent geometric imperfections based on the recommendation of EN 1993-1-5 for flat web girders can lead to consequently lower buckling resistance than imperfections based on virtual manufacturing in the case of the analysed girders. It is demonstrated that the application of virtual manufacturing and virtual testing may ensure increased shear buckling resistance in advanced design. Reason of the obtained trend is that residual stresses are negligible in the web of corrugated web girders; in addition, magnitude of initial geometric imperfections in the web is generally much smaller than permitted manufacturing tolerances for plate curvature and web distortion in the standard. However, standard-based equivalent geometric imperfection does not consider this specialty of corrugated web girders. Related publications: **[DK3] & [DK8]**

using a three-dimensional heat transfer model and Goldak's double ellipsoidal heat source model for a metal active gas welding power source. Fusion zone sizes and residual deformations are predicted in T-joints with fillet and groove welds in S355J2+N structural steel weldments using a mixture of argon and carbon dioxide as shielding gas, PA flat or PB horizontal-vertical welding positions and two different electrode types, namely solid wire and flux cored electrodes. The developed weld process model is novel in terms of describing the relationship between net heat input and heat source model parameters.

Related publications: **[DK1] & [DK7]**

Thesis 3. An experimental research program is conducted in order to measure total strains during welding of corrugated web girders having three different corrugation profiles. The following conclusions are drawn based on the measurements:

a) Trapezoidal geometry of the web results in alternating torsion and out-of-plane bending about the vertical and longitudinal axes during welding, that reduces local and global deformations of trapezoidal web girders in comparison to conventional I-girders.

b) Total strain differences on inclined and parallel folds are not dominant due to out-of-plane bending about the longitudinal axis as the deformation is not prevented in the vertical direction, except by the bending stiffness of the flanges.

c) Total strain differences on parallel folds are dominant due to out-of-plane bending about the vertical axis; the larger the corrugation angle θ the smaller the derived strain difference; increase in bending stiffness EI_z of inclined folds about global longitudinal axis results in reduced curvature.

d) Total strain differences on inclined folds are not relevant due to out-of-plane bending about the vertical axis as shear strains dominate.

Related publications: **[DK2] & [DK8]**

Thesis 4. Finite element model for welding simulation of corrugated web girders is validated based on the evolution of total strains by laboratory test results. The following conclusions are drawn based on the numerical simulation results:

a) Typical welding-induced longitudinal residual stress distributions in the web and flanges of corrugated web girders are determined and compared with residual stress pattern proposal from literature and residual stress patterns specific for conventional

3 Development of finite element framework

3.1 Welding simulation

A complex modelling framework, including three-dimensional transient thermo-metallurgical-mechanical, uncoupled thermo-mechanical analyses and simplified welding simulation techniques, have been developed in ANSYS to simulate fusion welding processes in order to determine and evaluate temperature fields, analyse the evolution of welding-induced strains and stresses, residual stresses and deformations. The developed approach was validated based on temperature and residual stress measurements. Generally, uncoupled thermo-mechanical analyses are performed in the thesis, however, the possibility of running a thermo-metallurgical-mechanical analysis is developed as well. Validation of thermo-metallurgical-mechanical analysis is based on numerical results of a welding simulation software package. Three-dimensional transient analysis is performed for detailed calculation purpose, which is a comprehensive technique for welding simulations. Generally, it can be declared that modelling large scale welded structures with transient heat source is nearly impossible with acceptable computational time. Simplified approaches such as lump-pass analysis are also implemented.

The developed numerical framework utilizes solid elements regarding the complexity of the problem. Generally, finite elements of the same order are used in thermal and mechanical analyses, while linear elements are recommended in welding simulations as smaller low-order elements perform better than larger high-order elements in nonlinear problems. Nevertheless, linear elements require reduced integration of volumetric strain fields in order to prevent volumetric locking when there are large plastic strains. SOLID70, a thermal solid element, has a three-dimensional thermal conduction capability. The element has eight nodes with a single thermal degree of freedom at each node. SOLID185, the equivalent structural solid element, has eight nodes with three translational degrees of freedom (in nodal x, y, and z directions) at each node. Solid elements with pure displacement formulation and full integration with B-bar method (also known as selective reduced integration method) are used in the vicinity of the weld. Elements with enhanced strain formulation are applied in the remaining domains.

Thermal and mechanical material properties are based on EN 1993-1-2 in the thermo-mechanical analysis. The standard uses reduction factors for defining temperature-dependent Young's modulus, yield strength and stress-strain curves. A multilinear isotropic hardening model is used in the simulations with von Mises yield criterion and associative flow rule.

The developed method for filler material addition in ANSYS is a combination of quiet element technique and inactive element technique. The inactive element technique ('birth and death' procedure) is used in the thermal analysis. In the mechanical analysis, the quiet element technique is implemented, since all elements are active from the beginning of the calculation. Young's modulus of 1000 MPa is used for not yet deposited or melted material, while linear thermal expansion coefficient is taken as zero to ensure thermal strain free bead elements before welding.

Goldak's double ellipsoidal heat source model is implemented in the numerical framework. In general, movement of heat sources is modelled using local coordinate systems (LCSYS). The LCSYS centre represents the instantaneous position of the welding torch, while absorbed heat due to welding is generated in the workpiece regarding the heat source model and the distances from the centre. Since welding trajectories and LCSYS positions cannot be described using equations in most of the cases, an automated Frenet-Serret frame is developed to simulate every possible trajectory. **Figure 1** shows temperature fields during welding specimens with one-, two- and three-dimensional trajectory (1D, 2D and 3D, respectively) using the developed automated Frenet-Serret frame algorithm. In addition, travel speed, i.e., heat input, is automatically modified (linearly changed) depending on the reference and actual cross-sectional area for each weld pass. It is beneficial and reasonable to have the possibility of modulating heat input in the case of three-dimensional welding trajectories where fillet size varies along the trajectory (e.g., **Figure 1c**).

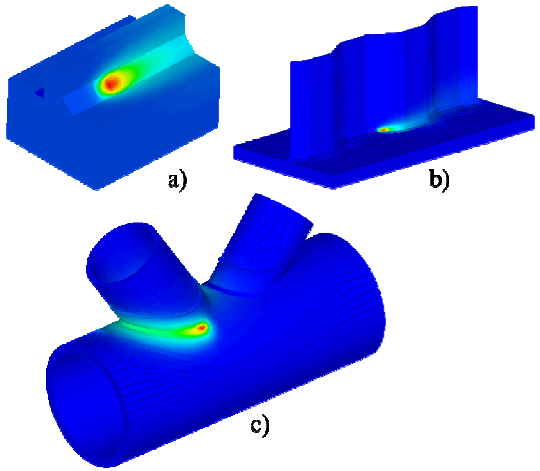

Fig. 1 Schematic temperature fields during welding of a) a T-joint (1D trajectory), b) a corrugated web girder (2D trajectory) and c) a CHS K-joint (3D trajectory) using the developed algorithm.

testing may ensure extra strength in the design phase. Thus, application of equivalent geometric imperfections gives conservative results for the investigated geometries. The simulated shear buckling resistances are compared with previously developed design formulae. Design formulae recommended by the EN 1993-1-5 provide conservative resistances for all the four studied configurations. Results also show that application of equivalent geometric imperfections results in significantly smaller shear buckling resistance than using realistic imperfections, which highlights the advantage of the presented advanced calculation method. Shear buckling resistance determined by a numerical model using equivalent geometric imperfections leads to resistances close to the prediction of EN 1993-1-5, which clearly shows the overestimation of the reduction effect of residual stresses and geometric imperfections on the resistance of girders with corrugated web. It can be also observed that formulae taking interactive buckling into account give similar resistance values as virtual testing.

6 New academic contributions

6.1 Theses of the dissertation

Thesis 1. A computational framework is developed and validated in a general-purpose finite element environment for simulating arc welding processes in order to predict microstructural changes, temperature, stress and deformation fields of steel structures during welding. Uncoupled transient thermo-metallurgical-mechanical analyses are implemented for virtual manufacturing. The novelty of the framework compared to other welding simulation software packages is a built-in automated Frenet-Serret frame, which is developed and verified in order to simulate any arbitrary three-dimensional welding trajectory and movement of a local coordinate system representing the current location of the heat source. Heat input is automatically modified by using this technique depending on the reference and actual cross-sectional area of each weld pass during thermal analysis in accordance with the basics of weld seam tracking techniques for robotic welding.
Related publications: **[DK1] – [DK3]**

Thesis 2. A novel weld process model, focusing on modelling the physics of heat generation, is developed and validated based on large number of experimental data

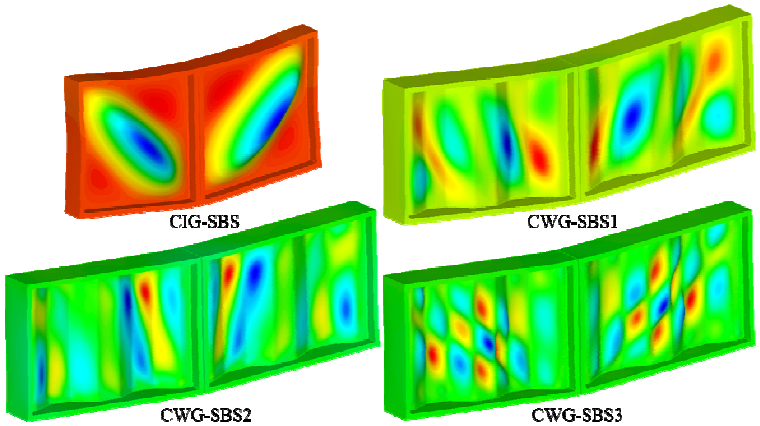

Fig. 18 Computed failure modes (out-of-plane deformation).

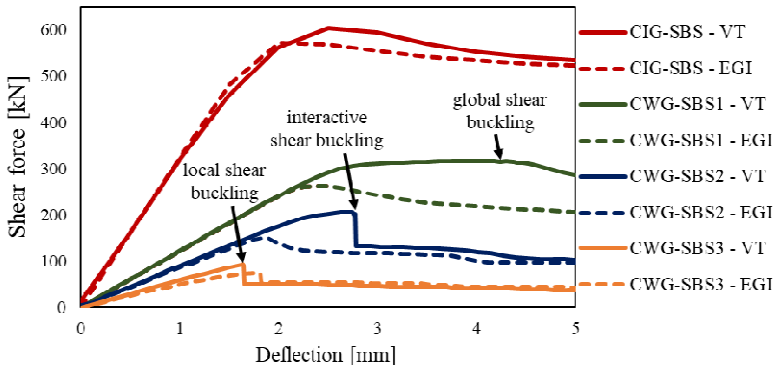

Fig. 19 Reaction force – vertical displacement curves.

The simulated shear buckling resistances using equivalent geometric imperfections (h_w/200) are consequently lower than the buckling resistances based on virtual testing of previously manufactured specimens for the selected geometries as it is shown in the shear force – vertical displacement curves. In general, residual stresses are negligible in the web of corrugated web girders as shown previously. In addition, the magnitude of the real initial geometric imperfections in the web is usually much smaller than permitted manufacturing tolerances for plate curvature (h_w/80) and web distortion (h_w/100) in EN 1090-2. Increasing the web thickness results in higher shear buckling resistance. The applicability of equivalent geometric imperfections based on the recommendation of EN 1993-1-5 for flat web girders is presented; however, virtual manufacturing and virtual

3.2 Geometrically and materially nonlinear analysis with imperfections

Virtual testing of previously manufactured specimens is an advanced application in manufacturing and design. The developed approach for virtual testing of manufactured specimens is illustrated with an example in **Figure 2**. The figure shows von Mises residual stresses of a trapezoidal corrugated web girder after each step of the manufacturing process, (i) cold forming, (ii) thermal cutting and (iii) welding. Detail (iv) represents the redefined loads and boundary conditions during virtual testing. Plane symmetry is assumed, while displacement load is applied in the plane of symmetry to model the typical experimental set-up of shear buckling tests of short, simply supported girders. Finally, von Mises stresses, including residual stresses, are shown at (v) shear buckling failure. The material model is identical in virtual manufacturing and virtual testing. Large deflection effects are included in the static analysis. Sparse solver is used with full Newton-Raphson method updating the stiffness matrix at each equilibrium iteration. Line search option is activated to improve Newton-Raphson method. Stress stiffening effects are automatically included in all geometrically nonlinear analyses. Automatic time stepping is turned on to control incremental force-controlled or displacement-controlled loading. The numerical approach is validated using experimental and numerical flexural buckling resistances of a box section column; results are compared and obtained difference is less than 2% by using real material properties based on tensile tests.

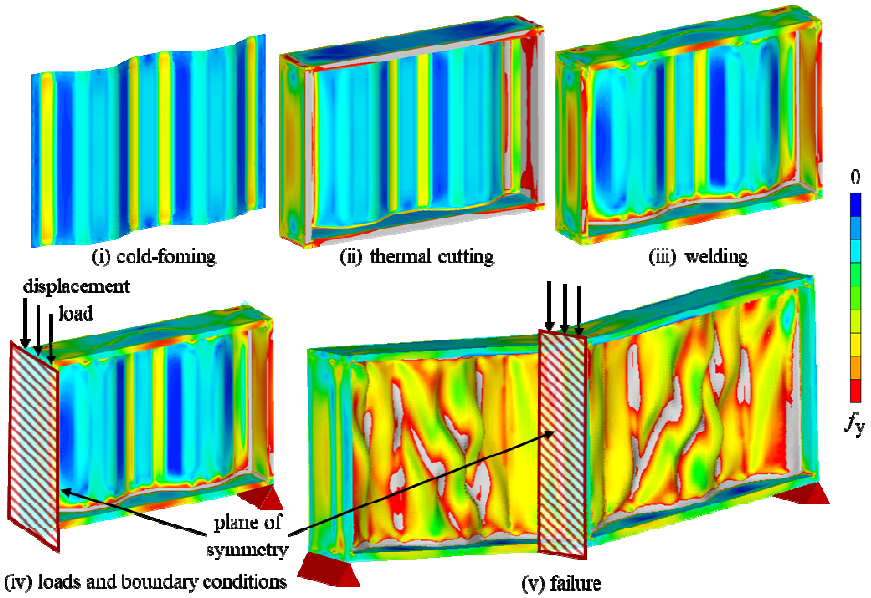

Fig. 2 Steps of the developed approach for virtual testing of specimens.

4 Development of weld process model

A weld process model, focusing on modelling the physics of heat generation, is developed which uses a three-dimensional heat transfer model and Goldak's double ellipsoidal heat source model for a metal active gas welding power source. The current research program contains (i) literature review focusing on weld heat source model generations and accompanying phenomena taken into consideration, (ii) a systematic experimental study of small-scale test specimens using different welding variables, (iii) numerical investigations using transient uncoupled thermo-mechanical analysis for virtual manufacturing, (iv) a parametric study of welding variables and heat source model parameters using numerical simulation and (v) validation of the developed weld process model based on experimental results.

Small-scale welded T-joints of a stator segment of a wind turbine are investigated in the current research work. The major aim of the experimental research program is to evaluate the effects of different filler metals, welding variables and types of welding joints on manufacturing productivity and structural behaviour. High-cycle fatigue is crucial in the case of wind turbines; therefore, three weld types are analysed (**Figure 3**) having considerably different resistance against cyclic loading: (a) double-bevel groove weld, (b) double-sided fillet welds and (c) single-bevel groove weld.

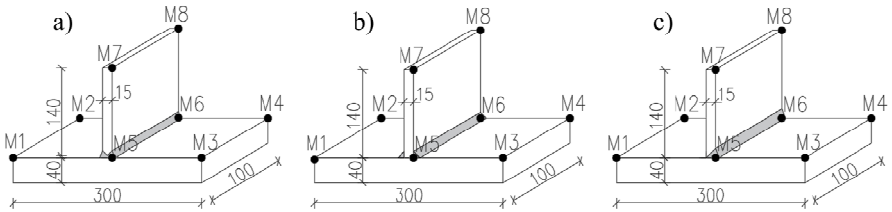

Fig. 3 Types of investigated T-joints: a) double-bevel groove weld, b) double-sided fillet welds and c) single-bevel groove weld.

A number of weld passes and heat input are the investigated variables resulting in a database of input parameters including the cross-sectional area of the fusion zones. Fusion zone size is measured after manufacturing using macrographs. These measurements are the basis of the heat source model validation process. The initial and deformed configurations of the joints are measured with a coordinate-measuring machine at specific points, denoted by M1-M8 in **Figure 3**, thus, welding-induced deformations can be calculated after using coordinate transformations. Vickers hardness

The sizes of tensile zones near the weld are nearly the same (~15-20 mm→~4-5 t_w). Significant compressive residual stresses (~70-200 MPa) appear around 20-25 mm (~5-6 t_w) from the web-to-flange joint. However, nearly zero (~5-30 MPa) compressive and tensile stresses are present in the middle of the corrugated webs, while only compressive stresses (~60 MPa) are typical in this region for the I-girder. It can be concluded based on the numerical simulations that corrugation angle and thermal efficiency may have a large influence on residual stresses in the web; characteristic heat source model parameters are of minor importance.

Averaged longitudinal residual stresses in the flanges due to welding are shown in **Figure 17**. The magnitude of compressive stresses is ~90-100 MPa in the flanges for the I-girder. Variation of corrugation angle results in shift of maximum tensile residual stresses as the plane of the subpanel is changing. Welding-induced transverse bending moment results in compressive (max.~100 MPa) and tensile stresses (max.~180 MPa) on the edges of the flange far from the weld. Tensile stresses increase as corrugation angle increases, while compressive stresses increase simultaneously on the other edge of the flange. Size of tensile zones near the weld are nearly the same (~25-28 mm→~2.5-2.8 t_f) for all the investigated cases, even for the I-girder with flat web. Generally, it can be observed, that welding results in mainly membrane residual stresses in case of flat web girders. However, bending residual stresses are dominant in case of corrugated web girders, and axial membrane residual stresses are significantly smaller in the web. Additional transverse bending moment can be also obtained in flanges in case of corrugated web girders, which is also a specialty of this girder type. Corrugated profile results in asymmetric residual stress pattern within the cross-sections, while increase in the corrugation depth results in larger bending residual stresses in the flanges.

Two geometrically and materially nonlinear analyses with imperfections are carried out for each geometry when analysing the shear buckling behaviour. The first analysis for each geometry applies the approach using equivalent geometric imperfections (EGI). Local out-of-plane imperfections with a magnitude of $h_w/200$, corresponding to the first eigenshape (shear buckling) using linear bifurcation analysis, are defined. The second analysis for each geometry uses the residual stresses and initial geometric imperfections (due to cold forming, thermal cutting and welding) provided by the previous virtual manufacturing process. The material model of steel is identical in the simulation of manufacturing and virtual testing (VT) as well using nominal material properties. Failure modes of virtually manufactured specimens are shown in **Figure 18**, while the corresponding shear force – deflection curves of the investigated girders are shown in **Figure 19**. Global, interactive and local shear buckling govern the failure of the investigated corrugated web girders CWG-SBS1, CWG-SBS2 and CWG-SBS3, respectively.

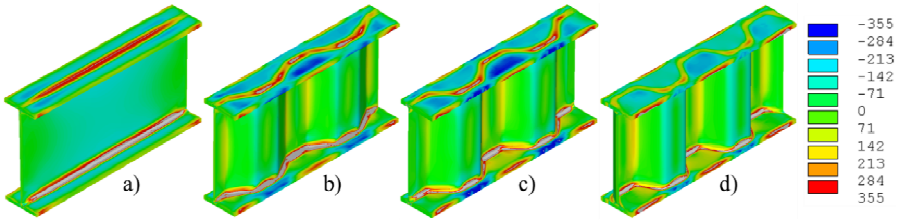

Fig. 15 Longitudinal residual stresses in [MPa] of a) a conventional girder with I-section and girders with corrugation angles of b) 30°, c) 45° and d) 60°.

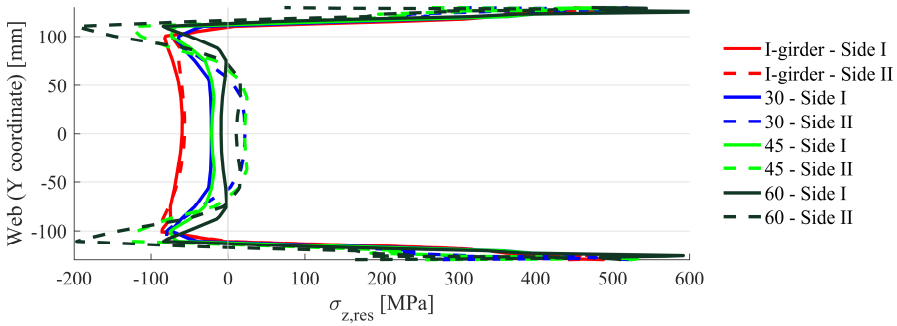

Fig. 16: Longitudinal residual stress distribution in the web using different corrugation angles.

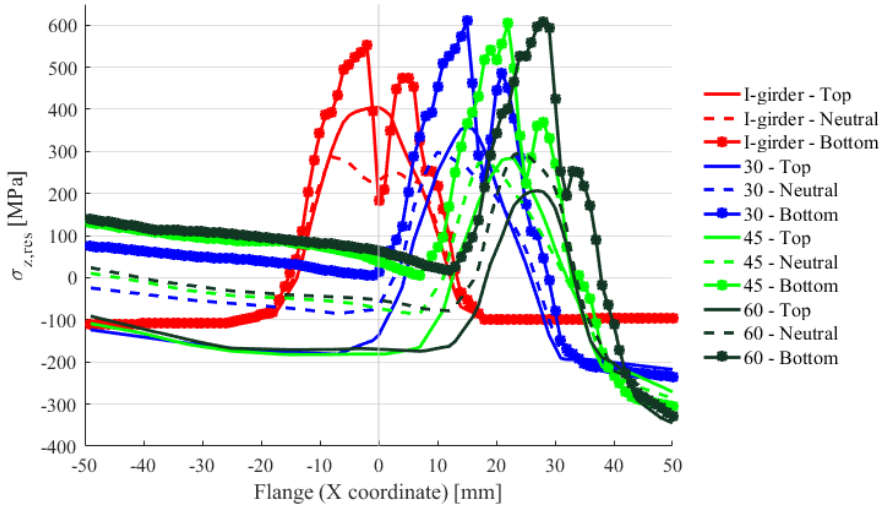

Fig. 17: Averaged longitudinal residual stress distribution in flanges using different corrugation angles.

tests, microstructural analyses and temperature measurements during welding are also carried out. All the specimens have a length of 100 mm. Steel base plates are manufactured with dimensions of 300 mm × 100 mm × 40 mm, while stiffeners are 140 mm × 100 mm × 15 mm. Plasma cutting is used for cutting the plates. Steel grade is S355J2+N for base plates and stiffeners as well. Macrographs are presented in **Figures 4 – 7**.

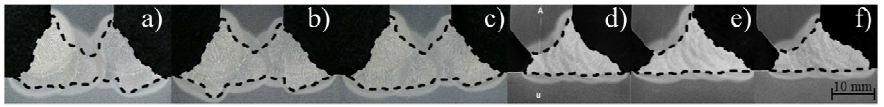

Fig. 4 Macrographs of double-bevel groove welds: a-c) JT1-1-01 – JT1-1-03 and d-f) JT1-2-01 – JT1-2-03.

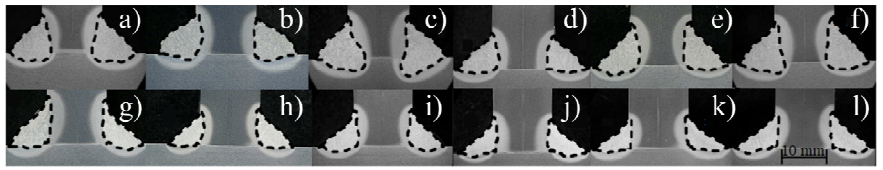

Fig. 5 Macrographs of double-sided fillet welds (single-pass welding): a-f) JT2-1-01 – JT2-1-06 and g-l) JT2-2-01 – JT2-2-06.

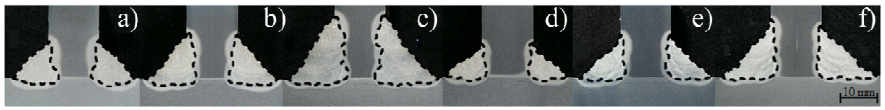

Fig. 6 Macrographs of double-sided fillet welds (multi-pass welding): a-c) JT2-1-07 – JT2-1-09 and d-f) JT2-2-07 – JT2-2-09.

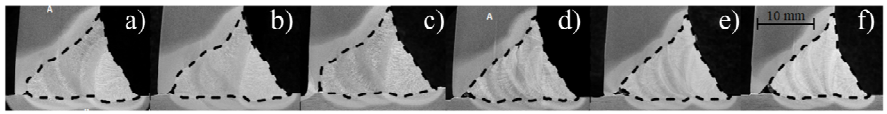

Fig. 7 Macrographs of single-bevel groove welds: a-c) JT3-1-01 – JT3-1-03 and d-f) JT3-2-01 – JT3-2-03.

The weldments are manufactured in PA flat or PB horizontal-vertical welding positions by using a Fronius TransPuls Synergic 5000 welding power source for metal active gas (MAG) welding using constant-voltage (slightly drooping) characteristics. Direct current and reverse polarity (DC+) are applied for the current applications. Welding current (I) and voltage (U) are registered during welding. Thus, operating points for each weld pass, assuming that arc length is constant, can be determined for configurations with solid wire and flux cored electrodes as arc characteristics for different filler metals, wire diameters and shielding gases are distinct. The solid wire electrode is Esab OK Aristorod 12.50 (EN ISO 14341-A G 42 4 M G3Si1) and the flux cored electrode is Böhler Ti52 T-FD (EN ISO 17632-A T 46 4 P M 1 H5). The diameter of electrodes is 1.2 mm, while shielding gas is EN ISO 14175 - M21 - ArC – 18 and gas flow rate is 12-15 l/min. Temperature-indicating crayons are used for ensuring preheat and interpass

temperatures which are both 150 °C. Ambient temperature is between 20-22 °C during the experiments. The total heat input varies between 0.60 and 2.71 kJ/mm depending on filler metal, weld type and number of passes. In total, eighty-two weld passes are laid using solid wire electrodes and eighty-one weld passes are carried out applying flux cored electrodes. Hence, the number of data points is equal to the number of weld passes in **Figure 8**. A linear regression analysis is carried out using the least squares method to determine the welding current-voltage relationship for globular and spray arc metal transfer modes, marked with continuous solid lines, for both electrodes. Error bars are denoting standard deviations of discrepancies (s = 0.81 V and s = 0.38 V), for solid wire and flux cored electrodes, between measured data and corresponding values of the regression line representing the uncertainties in arc characteristic ranges, i.e., increase and decrease of contact tip-to-workpiece distance and arc length. The current-voltage equations for the solid wire and flux cored electrodes are shown in the figure representing the operating points after linear regression analysis. These equations can be applied in the preliminary design phase when calculating heat input. In addition, they are implemented in the numerical model developed for the welding simulation of T-joints.

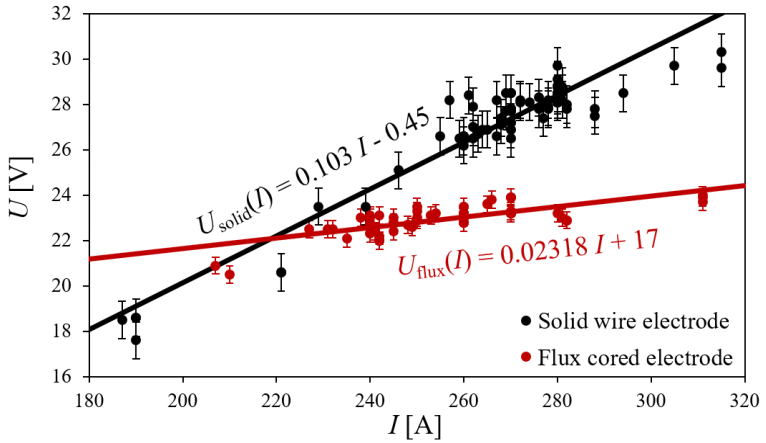

Fig. 8 Operating points and the relationship between current and voltage for solid wire and flux cored electrodes.

First, thermal efficiency is determined by the comparison of experimental and numerical data as presented in **Figure 9** showing time-temperature curves based on infrared thermal imaging ('Measurement') and finite element analysis ('FEA'). The peak temperature is approximately 700-800 °C for both cases and the cooling phenomenon is also simulated accurately. The temperature is about 200 °C at 200 s in the case of the investigated configurations for both approaches. The figure presents the macrograph of specimen JT2-1-06

The variation of total strain differences ($\Delta\varepsilon_{tot}$) in time, derived from opposite strain gauge measurements (positive differences due to positive bending about local Y and Z axes) are presented in **Figure 13**. Legends in both figures use the following notations (e.g., H-I-30): H/V – horizontal/vertical strain gauge, I/P – location of the strain gauge; middle of an inclined/parallel fold, 30/45/60 – corrugation angle in degrees. Total strain differences $\Delta\varepsilon_{tot,z}$ derived from horizontal strain gauges show that increasing corrugation angle results in reduced deformations due to bending about local Y axis in parallel folds, while bending does not have a large influence in case of inclined folds. Bending about Z axis results in total strain differences $\Delta\varepsilon_{tot,y}$ derived from vertical strain gauge results. However, based on the test results it has only minor influence.

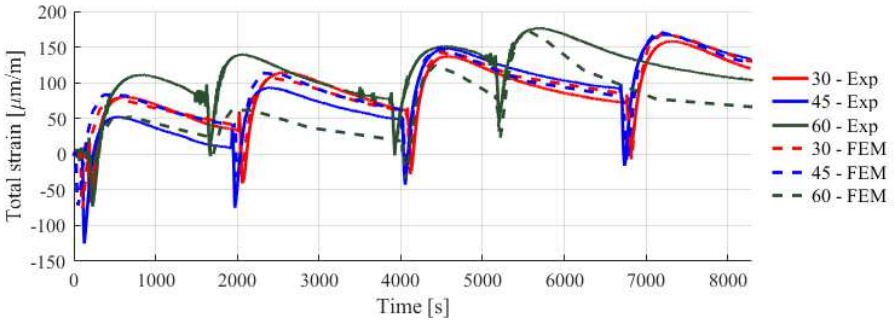

Fig. 14 Evolution of total strains based on measurements ('Exp') and simulation ('FEM').

Validation of the developed numerical model for welding simulation of corrugated web girders is presented. **Figure 14** shows the total strains measured by strain gauges ('Exp') and computed results using finite element method ('FEM'). Results refer to the centre of subpanels in the middle section of the analysed girders. The comparison of experimental and numerical data shows good agreement for all the three analysed corrugation angles (30°, 45° and 60°). Effect of different heat source model parameters and heat inputs on total strains has been investigated in a numerical parametric study. Heat source parameters do not have a large influence (maximum of 25 μm/m in case of lack of fusion), while 25% change in heat input could result in 55 μm/m variance in total strains. The maximum difference is observed for girder with corrugation angle of 60°, which is 75 μm/m and it is within the tolerance according to the numerical parametric study.

Longitudinal residual stresses in flat web and corrugated web girders are shown in **Figure 15** taking cold forming (if any), thermal cutting and welding into account. Longitudinal residual stresses in the web due to welding are shown in **Figure 16**.

used for metal active gas (135 MAG) welding during manufacturing. PB horizontal-vertical welding position is used for the fillet welds. The applied nominal welding variables are the following: voltage is 32.6 V, current is 259 A, while wire feed speed is 6 m/min and gas flow rate is 12-15 l/min. Average travel speed is between 9.0-11.1 mm/s, 9.3-10.4 mm/s and 7.9-8.5 mm/s for specimens with corrugation angle of 30°, 45° and 60°, respectively. These inputs result in a total heat input of 0.76-0.93 kJ/mm, 0.81-0.91 kJ/mm and 0.99-1.07 kJ/mm, respectively. Temperatures are nearly the same at the installed opposite strain gauges far from the welds; therefore, it makes it possible to filter out thermal strains when calculating elastic strains due to out-of-plane bending. Strain measurements are used for drawing conclusions regarding the influence of corrugation angle via total strain difference curves and to validate the finite element model developed for welding simulation of corrugated web girders.

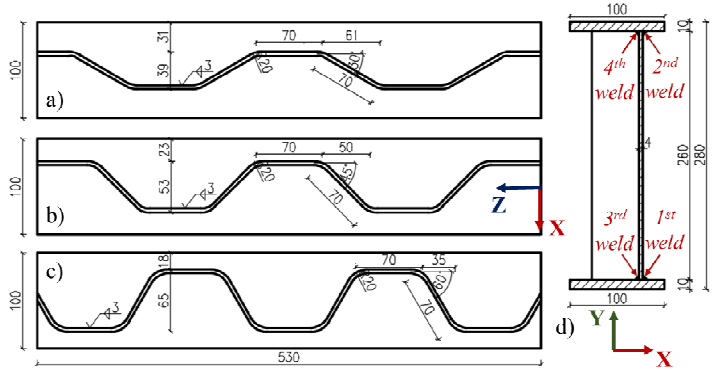

Fig. 12 Specimen geometries with corrugation angles of a) 30°, b) 45° and c) 60°.

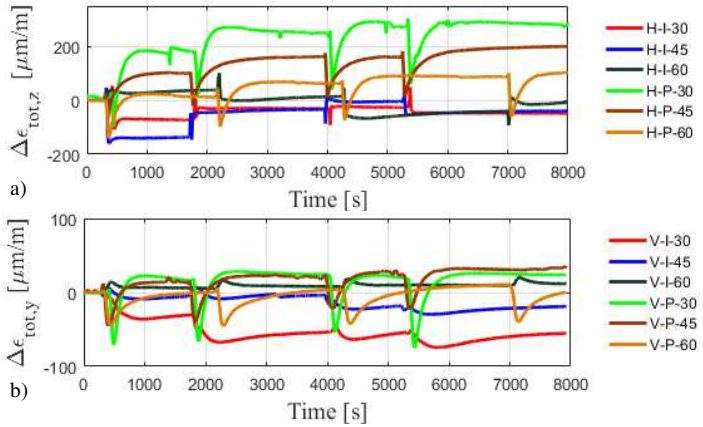

Fig. 13 Total strain differences derived from strain gauge measurements: a) horizontal ($\Delta\varepsilon_{tot,z}$) and b) vertical ($\Delta\varepsilon_{tot,y}$) strain gauges for corrugation angles of 30°, 45° and 60°, respectively.

as well and a cross-section of the finite element model denoting the fusion zone. Calibration is based on fusion zone size. The aim is to approximate the measured fusion zone size within an arbitrary ±10% range specified for handling uncertainties in welding variables. The cross-sectional areas of the fusion zones for specimen JT2-1-06, by measurements, are 75 mm^2 and 74 mm^2 for the 1st and 2nd weld beads, respectively. In addition, fusion zone sizes are 43 mm^2 and 39 mm^2 for specimen JT2-2-02. The corresponding simulated weld pool sizes are 68 mm^2, 67 mm^2, 42 mm^2 and 37 mm^2, respectively, which shows good agreement. Thermal efficiency η of 0.90 is accepted related to the comparison of numerical and experimental data and it is applied in the simulations hereafter for both electrodes.

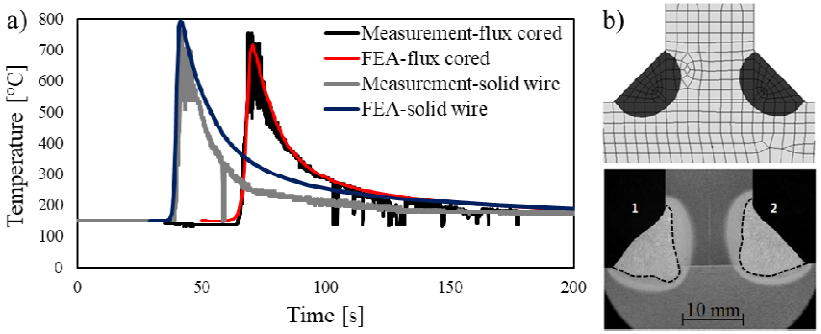

Fig. 9 Determination of thermal efficiency by a) temperature measurements for flux cored and solid wire electrodes and b) a macrograph of specimen JT2-1-06.

Furthermore, characteristic parameters of the implemented double ellipsoidal heat source model are calibrated for a typical range of welding variables in the case of double-sided fillet welds with single weld passes. A total of twelve specimens are modelled in the numerical research program. Double-sided fillet welded T-joints with single pass welds are investigated. The actual dimensions of the joints are modelled with the corresponding fillet sizes. Voltage is calculated using equations in **Figure 8** depending on the type of filler metal. After performing dozens of iterations, a function of heat input is developed to evaluate a and b characteristic parameters of Goldak's double ellipsoidal heat source model. An $a(q_{net})$ polynomial function is determined for flux cored electrodes. The model for this configuration assumes that $a = b$ and $c_r = c_f = 2.5$ mm regarding previous simulations of the joints. The characteristic parameters of Goldak's double ellipsoidal heat source model are independent of the net heat input q_{net} for the configurations welded with solid wire electrode ($a = b = 10$ mm and $c_r = c_f = 2.5$ mm). Obviously, small c_r and c_f parameters result in a requirement of dense mesh along welding trajectory. Minimum and maximum errors are -

9.9% and 9.8%, while the mean and standard deviation of errors are -1.9% and 6.0%, respectively. The calibrated parameters for double-sided fillet welds with single weld passes are validated using an extended set of parameters in the case of the three types of T-joint; one from each configuration is presented. **Figure 10** shows the finite element models and welding sequences of the weldments contributing in the validation process.

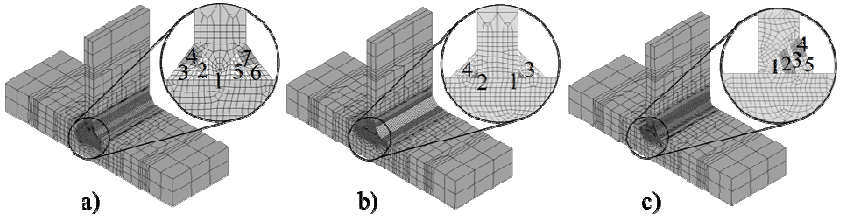

Fig. 10 Finite element models of a) JT1-1-03, b) JT2-1-07 and c) JT3-2-01.

Figure 11 shows the simulated fusion zones and the macrographs highlighting fusion lines with dashed lines; liquidus temperature is assumed to be 1500 °C. Measurements and numerical results are in a good agreement for the specimens, the absolute maximum error in the cross-sectional area of the fusion zone is 8.8%, which is a good approximation.

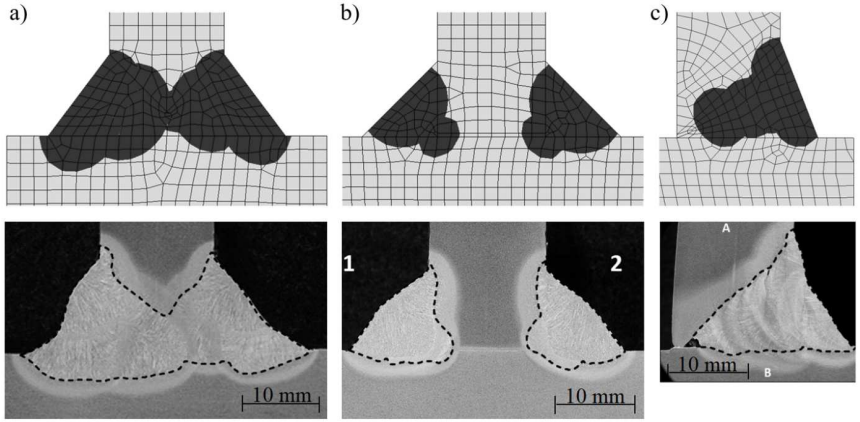

Fig. 11 Simulated and measured fusion zones for a) JT1-1-03, b) JT2-1-07 and c) JT3-2-01.

Transverse deformations are dominant for this joint type. Specimens a)-c) have maximum simulated transverse deformations of 2.19 mm (measurement: 2.80 mm), 1.02 mm (measurement: 1.53 mm) and 8.65 mm (measurement: 8.85 mm), respectively. Results show that the double-bevel groove weld and the double-sided fillet weld have performed well in a distortion-controlled design. Obviously, the T-joint with single-bevel groove weld is the worst configuration in this sense.

5 Virtual buckling tests of trapezoidal corrugated web girders

Application of corrugated web has significantly increased in the field of structural engineering in the past decades due to numerous favourable properties, especially in bridges (e.g., Maupré Viaduct and Dole Bridge in France, Hontani Bridge in Japan, Altwipfergrund Bridge in Germany and Móra Ferenc Bridge in Hungary, etc.). Residual stresses and initial geometric imperfections have important effect on the buckling resistance of slender plated girders. Corrugated profiles are stiffer during construction, and corrugation increases the buckling resistance of the web. Web stiffeners can be eliminated, or their number can be significantly reduced. Shear buckling resistance of conventional I-girders with flat webs have been extensively analysed previously. However, sensitivity of corrugated web girders to imperfections needs further investigations.

The aim of the current research program is (i) to conduct a literature review focusing on welding-induced residual stresses, welding simulations and shear buckling resistance regarding steel I-girders with flat and corrugated webs, (ii) to perform an experimental and numerical study focusing on the evolution of total strains in corrugated web girders, (iii) to validate the developed finite element model for welding simulations, (iv) to determine typical welding-induced longitudinal residual stresses in the web and flanges, (v) to compare residual stress pattern of corrugated web girders and conventional I-girders with flat web, (vi) to apply virtual manufacturing as an input, supplying residual stresses and deformations, for subsequent virtual testing in a geometrically and materially nonlinear analysis with realistic manufacturing-induced imperfections to determine the shear buckling resistance and (vii) to compare numerical results with previously proposed design approaches. The developed finite element model is able to virtually simulate the manufacturing process (cold forming, thermal cutting, welding) of corrugated web girders and it is capable of simulating thermal phenomena during manufacturing and predicting the influence of welding variables on imperfections and buckling resistance.

The analysed configurations are shown in **Figure 12**. The applied corrugation angles θ are 30°, 45° and 60° for the three type of specimens, respectively. Three specimens are manufactured for each corrugation profile. All the specimens are made from S355J2+N steel grade with a length L of 530 mm and a height of 260 mm. Flanges are manufactured from steel plates with dimensions of 100 mm × 10 mm ($b_f \times t_f$), web plates with dimensions of 260 mm × 4 mm ($h_w \times t_w$) are used, while fold lengths a_1 and a_2 are equal to 70 mm. Plasma cutting is used for cutting the plates. Double-sided fillet welds are laid with fillet size of 3 mm. A REHM Mega.Arc 450 welding power source, M21 - ArC - 18 (Corgon 18) shielding gas and Böhler EMK 8 solid wire electrode with a diameter of 1.2 mm are